Phospholipid Topography of Whole-Body Sections of the *Anopheles stephensi* Mosquito, Characterized by High-Resolution Atmospheric-Pressure Scanning Microprobe Matrix-Assisted Laser Desorption/Ionization Mass Spectrometry Imaging
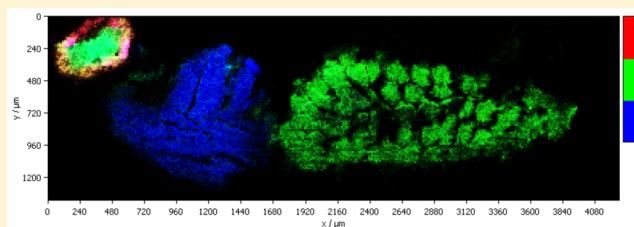
Saleh M. Khalil,[†] Andreas Römpp,[†] Jette Pretzel,[‡] Katja Becker,[‡] and Bernhard Spengler*,[†]

[†]Institute of Inorganic and Analytical Chemistry, Justus Liebig University Giessen, Heinrich-Buff-Ring 17, 35392 Giessen, Germany
[‡]Biochemistry and Molecular Biology, Interdisciplinary Research Center, Justus Liebig University Giessen, 35392 Giessen, Germany

Ⓢ *Supporting Information*

ABSTRACT: High-resolution atmospheric-pressure scanning microprobe matrix-assisted laser desorption/ionization mass spectrometry imaging (AP-SMALDI MSI) has been employed to study the molecular anatomical structure of rodent malaria vector *Anopheles stephensi* mosquitoes. A dedicated sample preparation method was developed which suits both, the special tissue properties of the sample and the requirements of high-resolution MALDI imaging. Embedding in 5% carboxymethylcellulose (CMC) was used to maintain the tissue integrity of the whole mosquitoes, being very soft, fragile, and difficult to handle. Individual lipid compounds, specifically representing certain cell types, tissue areas, or organs, were detected and imaged in 20 μm-thick whole-body tissue sections at a spatial resolution of 12 μm per image pixel. Mass spectrometric data and information quality were based on a mass resolution of 70 000 (at m/z 200) and a mass accuracy of better than 2 ppm in positive-ion mode on an orbital trapping mass spectrometer. A total of 67 imaged lipids were assigned by database search and, in a number of cases, identified via additional MS/MS fragmentation studies directly from tissue. This is the first MSI study at 12 μm spatial resolution of the malaria vector *Anopheles*. The study provides insights into the molecular anatomy of *Anopheles stephensi* and the distribution and localization of major classes of glycerophospholipids and sphingolipids. These data can be a basis for future experiments, investigating, e.g., the metabolism of *Plasmodium*-infected and -uninfected *Anopheles* mosquitoes.

Matrix-assisted laser desorption/ionization mass spectrometry imaging (MALDI-MSI) has become a prominent tool in bioanalysis, as it provides certain advantages over electrospray ionization (ESI) including tolerance to sample heterogeneity and spatial information.[1−4] Molecular topography and morphology provide valuable information about the function and properties of analytes, which is lost in typical MS measurements of homogenized samples. MALDI-MSI does not require labeling of targeted compounds and provides highly specific molecular information.[4] Lipids, neuropeptides, and drug compounds have been imaged in a wide range of biological samples at a spatial resolution down to 3 μm.[4]

In the present work, we used high-resolution atmospheric pressure scanning microprobe matrix-assisted laser desorption/ionization (AP-SMALDI-MSI) to detect and localize phospholipids and sphingolipids in various anatomical parts of the rodent malaria vector *Anopheles stephensi*, aiming to explore the lipid composition and distribution in the insect. The lipid-based biochemical pathways of the malaria parasite *Plasmodium* emerged as a potential target for drug discovery.[5−7] Knowledge of lipid biochemistry during mosquito stages of malaria parasites, however, is still rather limited.

Glycerophospholipids are the major structural lipids of cells and essential constituents of cell membranes, with phosphatidylcholines (PC) and phosphatidylethanolamines (PE). They are counting for more than half of the glycerophospholipids in eukaryotic membranes. Lysophospholipids (LPL), derivatives of phospholipids in which one or both acyl chains were removed by phospholipase A (PLA)-type enzymatic activity, were observed within the mass range of m/z = 400−600. LPLs have important signaling functions during inflammation, infection, injury, and other disease types.[8]

Malaria parasites utilize host phospholipids and modify the lipid content of host cells, as part of the pathophysiology of *Plasmodium* infection.[9,10] Therefore, the detailed characterization of the phospholipid topography of noninfected *Anopheles* mosquitoes is an excellent basis for systematically studying the lipid biochemistry of malaria infection, for further understanding parasite−host cell interaction and infection mechanisms as well as for identifying novel drug targets. Here, we describe the topographic characterization of specific
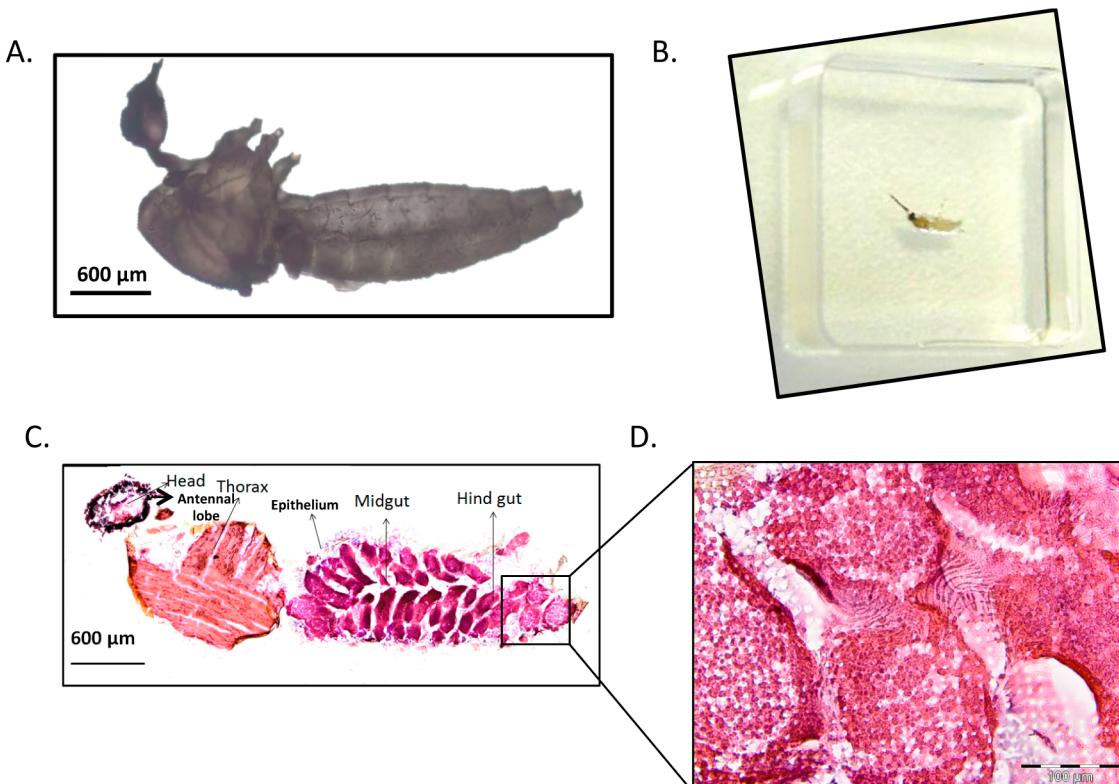
Figure 1. (A) Light microscopic image of a mosquito before sectioning. Wings and legs were removed. (B) Mosquito in a Cryomolds cast embedded in 5% CMC solution in the 15 mm × 15 mm × 5 mm square block. (C) Optical image of H&E-stained mosquito section (thickness, 20 μm) after MSI measurement. (D) Zoomed view after measurement of the gut region, showing the ablation spots (5 μm in diameter) and the spot distances of 12 μm.

phospholipid compounds in *An. stephensi*, the vector for rodent malaria.

■ MATERIALS AND METHODS

Chemicals. 2,5-Dihydroxybenzoic acid (DHB, 98% purity) was purchased from Fluka Sigma-Aldrich (Sweden). Glass microscope slides (ground edges frosted) were obtained from VWR International, Darmstadt, Germany, and carboxymethyl-cellulose (CMC) sodium salt from Sigma Life Science (USA). Trifluoroacetic acid (TFA) and water (HPLC grade) were purchased from Fluka (Neu Ulm, Germany). All chemicals used in this study were of highest purity available.

Instrumentation. An atmospheric pressure scanning microprobe matrix-assisted laser desorption/ionization ion source ("AP-SMALDI10", TransMIT GmbH, Giessen, Germany), coupled to a Fourier transform orbital trapping mass spectrometer ("Q Exactive", Thermo Fisher Scientific GmbH, Bremen, Germany), was used for imaging measurements with high resolution in mass and space.[11] In this setup, the laser beam is focused coaxial to the ion beam by a centrally bored objective lens to an optical diameter of 8.4 μm (1/e^2 definition), resulting in an ablation spot diameter of 5 μm under typical conditions. Samples were scanned with 12 μm steps within an area of 4.2 mm × 1.4 mm. The target voltage was set to 4.3 kV. With the AP-SMALDI10 ion source, a high spatial resolution of 3 μm (in oversampling mode) and 5 μm (in nonoversampling mode) from biological tissue sections has been reported.[4,12,13] The mass spectrometer was operated in positive-ion mode, and spectra were scanned in different mass ranges, varying from m/z 400 to 1 000. Automatic gain control

of the Q Exactive instrument was turned off. A matrix peak was used for internal "lock mass" calibration, resulting in a mass accuracy of better than 2 ppm over the entire image. Ions formed by 30 laser pulses per spot were accumulated in the C-trap prior to detection. The instrumental mass resolving power was set to 70 000 at m/z = 200 in centroid mode.

Cryosectioning of Anopheles. Female *An. stephensi* mosquitoes were frozen in liquid nitrogen 10 days after blood feeding and stored at −80 °C until cryosectioning.

A challenging part of our approach was the preparation of *Anopheles* sections for the imaging studies (Figure 1). Mosquitoes are small, soft, and fragile objects, making it impossible to obtain whole-body sections without suitable embedding. Preparation of the sections therefore had to be optimized systematically. We have tried several embedding materials like gelatin, tragacanth gum,[14] and carboxymethyl cellulose (CMC) to embed the mosquitoes at different dilutions (2−10%). It was found that for mosquito samples, 5% CMC embedding works best, as it can hold the integrity of the whole anatomy without breakage or distortion. Carboxymethyl cellulose also reduces the agility after covering the very fragile mosquito with embedding solution. CMC is readily available and easy to prepare compared to other reported embedding materials such as the synthesized polymer *N*-(2-hydroxypropyl) methacrylamide (pHPMA), which requires several synthetic reaction and purification steps.[15] Gelatin embedding (2−10%) has also been tested for the sectioning of Anopheles mosquitoes, as it was found advantageous for insects with hydrophobic hard cuticula.[16] For soft mosquito samples, however, embedding materials like gelatin and tragacanth gum
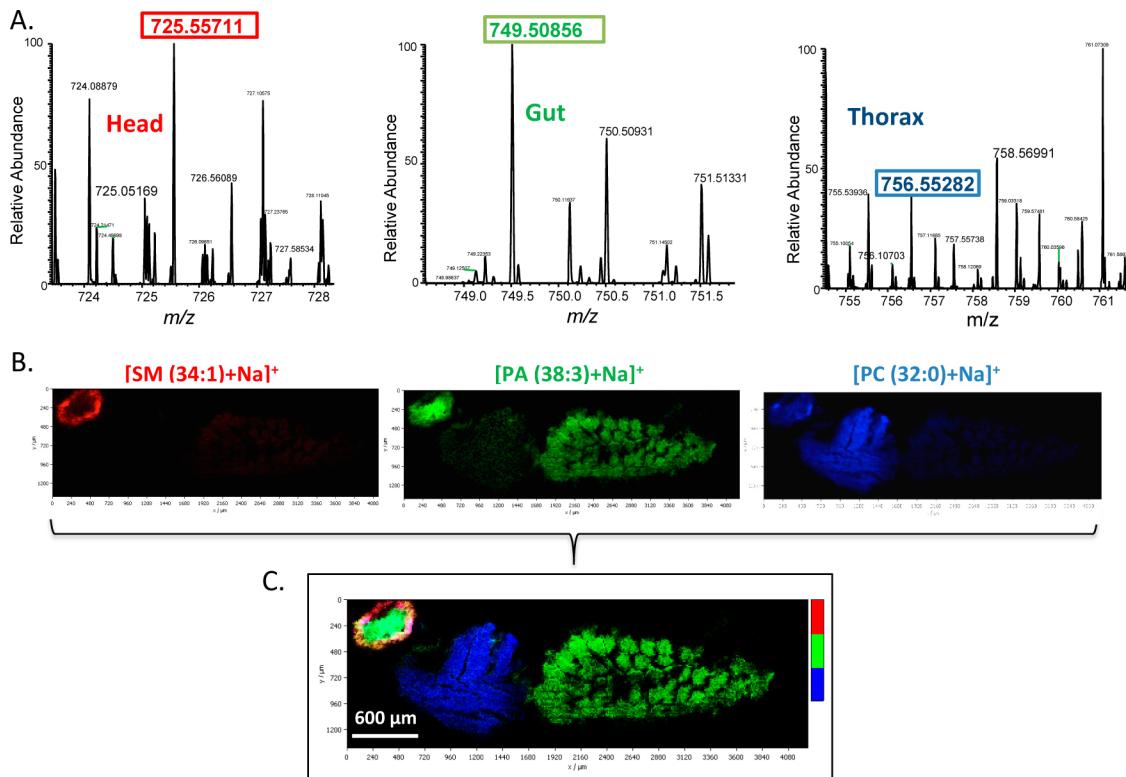
Figure 2. Positive-ion AP-SMALDI-MSI of glycerophospholipids and sphingolipids from an *An. stephensi* tissue section. (A) Positive-ion AP-SMALDI mass spectra averaged from head, gut, and thorax region of the mosquito section. (B) Positive-ion AP-SMALDI images of the [M + Na]$^+$ signals of sphingomyelin SM(34:1), phosphatidic acid PA(38:3), and phosphatidylcholine PC(32:0), generated with an imaging bin width of $\Delta m/z$ = 0.01 at a mass resolving power of 70000 at m/z 200 and a mass accuracy of better than 3 ppm. (C) Red-green-blue overlay image of the three selected lipid species.

were found incompatible to hold the integrity of the whole body and breakage was a common problem.

Legs and wings of the mosquitoes were removed before embedding, in order to obtain undistorted tissue sections. The detailed procedure of CMC embedding and sectioning of *An. stephensi* mosquitoes is described in the Supporting Information.

After embedding and freezing, tissue samples were cut in sections of 20 μm thickness with a cryotome (HM 525 Cryostat, Thermo Scientific, Dreieich, Germany) at −20 to −25 °C. The sections were thaw-mounted on glass slides and immediately measured or stored at −80 °C for later imaging studies. Before applying the matrix, the sections were put into a desiccator for 20 min to avoid condensation of humidity on the surface of the samples.

Matrix Application. For positive-ion measurements, DHB was homogeneously deposited by means of a pneumatic ultrafine sprayer ("SMALDIPrep", TransMIT GmbH, Giessen, Germany),[17] using 30 mg/mL of DHB in 50:50 (v/v) acetone−H_2O (0.1% TFA). The total volume of sprayed matrix solution was 200 μL and the spraying flow rate was 10 μL/min. Flow rate, N_2 pressure, and rotation of the sample probe were monitored throughout the spraying procedure. Before the tissue sections were analyzed, the resulting crystal size of the matrix on the tissue was controlled to be small (below 5 μm) and homogeneous, using a high-resolution optical microscope.

Optical Imaging. Optical images of *An. stephensi* sections of 20 μm thickness were taken with an Olympus BX-41X microscope (Olympus Europa GmbH, Hamburg, Germany)

after AP-SMALDI analysis, to correlate the anatomy with mass spectrometric images. For that, the matrix was removed from sections with 70% ethanol after being washed 10 min in a Petri dish. After matrix removal, sections were H&E-stained (Figure 1), as described in the Supporting Information (Table S3).

Data Processing. The in-house developed software package "MIRION" was used to generate mass images from raw files, acquired by the mass spectrometer with a bin width of $\Delta m/z$ = 0.01. Mass spectra from 5 μm spots within 12 μm pixels (sample steps) were obtained with a mass accuracy of ≤2 ppm (root-mean-square error). A typical red-green-blue (RGB) image of three selected lipid signals is shown in Figure 2.

Pseudocolor m/z images of individual lipid species were normalized to the highest intensity per image for each ion species. In order to compare abundances of lipids, the signals of protonated, sodiated, and potassiated species of each lipid were summed up and imaged as one image (Figure S1). No further data processing steps were applied during image generation.

Molecular Identification of Lipids through On-Tissue MS/MS Analysis. MS/MS analysis directly from *An. stephensi* tissue sections was performed using the Q Exactive orbital trapping mass spectrometer to confirm assignments and identify the major lipids, based on neutral losses and characteristic fragments of the head groups (Figure S3, Table S2). The selected precursor ions and the product ions obtained by high energy collision-induced dissociation (HCD) were ejected from the C-trap and mass analyzed. The normalized collision energy was set to 25%−30%, and positive fragment ions were detected in the orbitrap at a mass resolution set between 35 000 and 140 000 at a precursor isolation width of
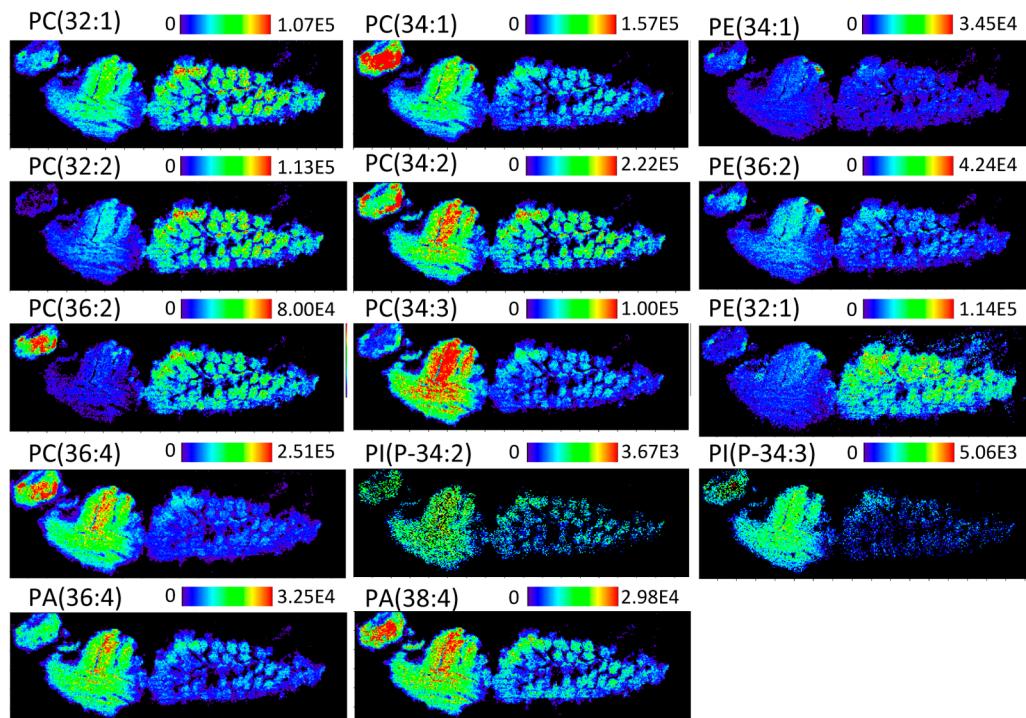
Figure 3. Positive-ion pseudocolor images obtained from the whole-body section of the mosquito. Relative abundances of phosphatidylcholines (PCs) and phosphatidylethanolamines (PEs) were found higher than other glycerophospholipid species, such as phosphatidic acid (PAs) and phosphatidylinositols (PIs). Phospholipid distributions correspond well with the anatomy of the animal. All images were created by adding signal intensities of the three ion species $[M + H]^+$, $[M + Na]^+$, and $[M+K]^+$ in one image.

± 0.5 u. In addition to the assignments based on accurate-mass analysis of the precursor ion, the on-tissue MS/MS analysis confirmed the assignment and allowed us to unambiguously identify specific lipid compounds.

RESULTS AND DISCUSSION

In this study, six classes of distribution patterns of glycerophospholipids and sphingolipids were determined using high-resolution AP-SMALDI-MSI in positive-ion mode in the mass range of $m/z = 400-1\,000$. High-resolution mass spectrometry imaging of *An. stephensi* determined lipid molecular species within discrete regions of tissues including head, thorax, midgut, and posterior midgut. A total of 67 different lipids could be assigned according to database searches (www.lipidmaps.org) within less than 2 ppm mass accuracy (Table S1). Reproducibility of distribution patterns was found to be very high, except for some expected preparation-dependent variation of signal intensities. As an example, Figure S5 shows phospholipid distribution patterns of two biological replicates for comparison for four selected phospholipid species.

Phospholipids in the following are reported with their overall carbon chain length sum and their degree of unsaturation, without specifying the individual acyl chains attached to the glycerol or sphingosine backbone.

The assignment of the lipid species was confirmed on the basis of protonated, sodium-, and potassium-attached monoisotopic lipid signals showing the corresponding distribution patterns. These three ion images were then combined into one pseudocolor image as the sum of the corresponding raw data signal intensities, in order to study the relative abundance of the lipids with a common scale. The images are reported here without specifying the nature of the acyl chains attached to the

lipids. Some of the abundant lipids were directly identified from tissue via tandem MS.

Regions of interest within the whole tissue section were assigned in an H&E-stained cryotome tissue section, representing the typical anatomical structural patterns of a 3.7 mm (h) × 1.2 mm (w) *An. stephensi* mosquito (Figure 1c).

As an example, the RGB overlay image of the lipid molecular ions at m/z 725.55711 ($[SM(34:1) + Na]^+$, red), m/z 749.50856 ($[PA(38:3) + Na]^+$, green), and m/z 756.55282 ($[PC(32:0) + Na]^+$, blue) qualitatively describes the distribution of these three particular lipids in the whole mosquito section. In particular, $[PC(32:0) + Na]^+$ was intensely observed in the head and thorax, $[SM(34:1) + Na]^+$ around the head, and $[PA(38:3) + Na]^+$ in the head and gut region (Figure 2).

Positive-ion data obtained from the AP-SMALDI-MSI experiments characterize the location and topography of glycerophospholipids in the various body regions of the vector *Anopheles*. Among these, phosphatidylcholines (PCs) and phosphatidylethanolamines (PEs) species were prominent compared to other lipids including phosphatidic acids (PAs), phosphatidylglycerols (PGs), and phosphatidylinositols (PIs). This is consistent with data from other insect species such as *Trogoderma granarium*[11] or subcellular fractions of *Aedes aegypti*.[18]

Identification and specific locations of lipid classes as well as characteristic compositions of anatomical regions and hot spots of the *Anopheles stephensi* mosquito are described in the following.

Phosphatidylcholines. The main lipid constituents of eukaryotic membranes are phosphatidylcholines (PCs), involved in the regulation of many cellular functions such as proliferation and differentiation. Spatial distribution of PCs on the molecular species level was determined from *An. stephensi*
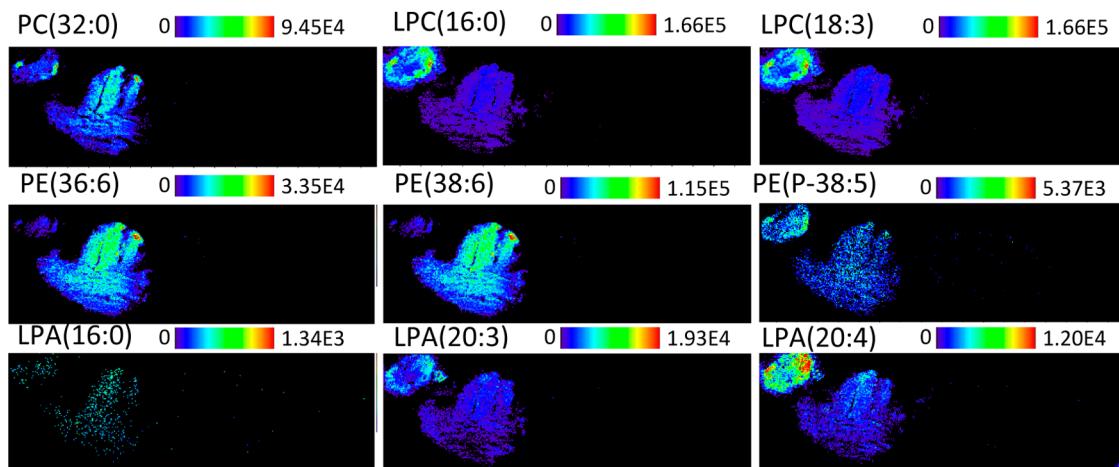
Figure 4. Positive-ion pseudocolor images of lipids found primarily in the <u>head and thorax</u> region. Major lipid species found here are PCs and PEs, along with enzyme-catalyzed lysophospholipids, LysoPCs, and LysoPAs.
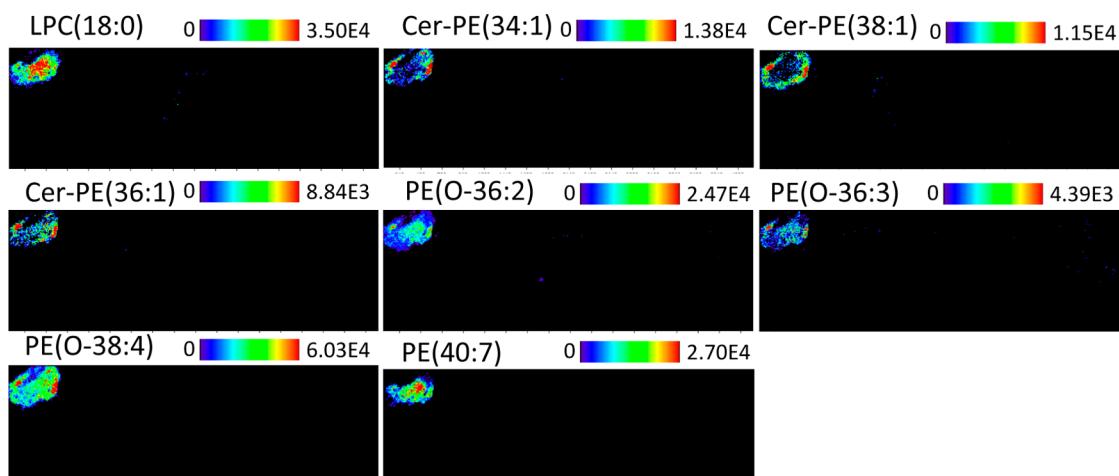

Figure 5. Positive-ion pseudocolor images of lipids found primarily in the <u>head</u> region. Major lipid species found here are ether lipids and sphingolipids, called ceramide-PE. The head region also contains PEs, PCs, LPCs, and PIs.

tissue sections and assigned according to sodiated, protonated, and potassiated species based on high mass resolution and high mass accuracy.

One of the most intense phospholipid signals was detected at m/z = 780.55155 with a mass error of 0.23 ppm, corresponding to sodiated PC(34:2). The positive-ion MALDI image of PC(34:2) (Figure 3) suggests that this phosphatidylcholine is distributed all over the tissue, observed in the head, thorax, and in the midgut and hind gut. The phospholipid was identified as PC(34:2) by on-tissue MS/MS analyses of the three ion species [M + H]⁺, [M + Na]⁺, and [M + K]⁺ (Figure S3A−C).

Positive-ion AP-SMALDI-MSI also revealed the presence of other phosphatidylcholines, such as m/z = 752.52037 identified as sodiated PC(32:2). The on-tissue MS/MS study resulted in characteristic product ions from the precursor phosphocholine headgroup at m/z = 693.44739 (neutral loss of 59, C_3H_9N), 569.45461 (neutral nonsodiated loss of 183), 547.47302 (neutral sodiated loss of 205), and adduct signature ion at m/z = 146.98192, resembling the characteristic sodiated species of unsaturated PC(32:2) (Figure S2), found to be distributed throughout the whole section with higher abundance in the gut region (Figure 3).

The signal of PC(34:3) was found to be rather intense in the thorax, while PC(34:1) was mainly observed in the head (Figure 3). Positive-ion AP-SMALDI-MSI also revealed the presence of other phosphatidylcholines, such as m/z= 754.53573, assigned as [PC(32:1) + Na]⁺, with the strongest intensities in the thorax and the gut, similar to the distribution of PC(34:2) (Figure 3). The on-tissue MS/MS study resulted in characteristic product ions at m/z = 146.98197, m/z = 571.47048 [M + Na − 183] and 695.46323 (neutral loss of phosphocholine 59, C_3H_9N), identifying the lipid ion species as sodiated monounsaturated PC(32:1) (Figure S3D). Saturated PC(32:0) was observed in the head and the thorax mainly (Figure 4 and Table S1).

Lysophosphatidylcholines. A prominent distribution of LPC(18:0) and LPC(20:5) was found in the head and antennal lobe (Figure 5 and Table S1), whereas LPC(16:0) was found in the head and the thorax (Figure 4 and Table S1). LPC(18:1) was found to be located in the head, thorax, and gut epithelial region (Figure 6 and Table S1), being the most intense LPC signal of this study. Identification of LPC(18:1) was performed via on-tissue MS/MS of m/z = 560.31110 directly from tissue, resulting in product ions at m/z = 162.95551, m/z =
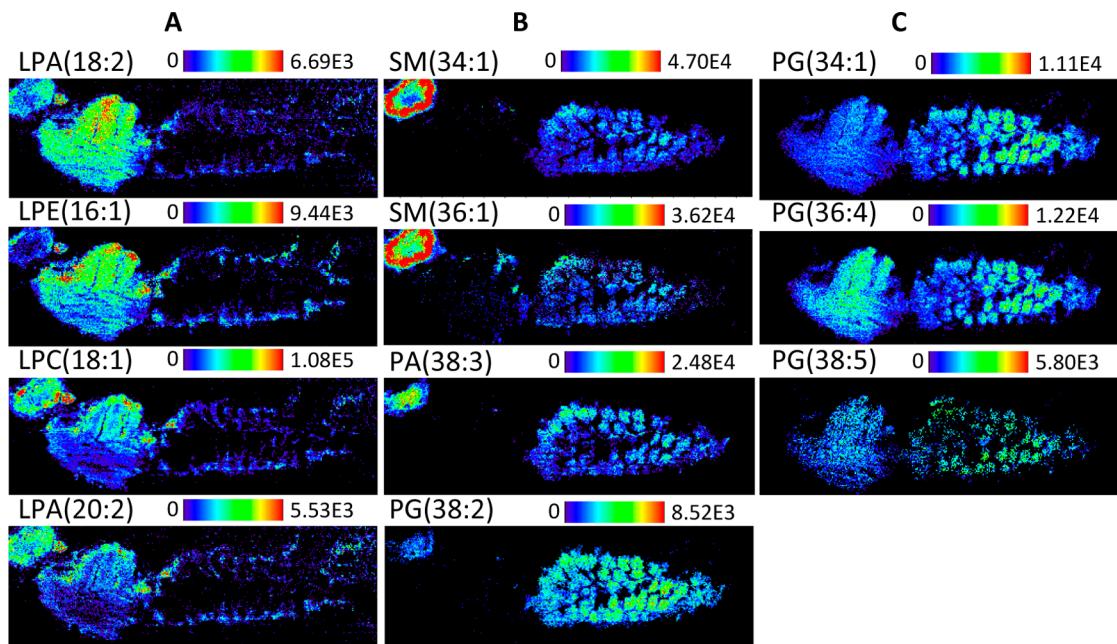
Figure 6. Positive-ion pseudocolor images of lipids (A) found primarily in the head, thorax and gut epithelium region, particularly rich in lysophospholipids LPCs, LPEs, and LPAs. (B) Images of lipids found primarily in the head and whole gut region. Two sphingomyelin lipid species were found with a similar distribution in these regions. Similar distribution patterns were observed for some other phospholipids. (C) Lipids found primarily in the thorax and gut region.

339.28873, and m/z = 501.23721, characteristic for the potassiated LPC(18:1) (Figure S3).

Phosphatidylethanolamines. Phosphatidylethanolamines (PEs) are the second most abundant phospholipid class found to be present in the mosquito. This is consistent with data from insect cell lines of *Spodopera frugipera* and *Trichoplusia ni*, where phosphatidylcholine and phosphatidylethanolamine were the major phospholipids.[19] PEs are main constituents of the architecture of biological membranes, being essential for membrane fusion and membrane curvature.[20,21] Furthermore, PEs are precursors for proapoptotic, anti-inflammatory, or signaling molecules (reviewed in ref 21). Figure 3 shows that the spatial distributions of PE(34:1), PE(34:2), and PE(36:2) were found rather homogeneously throughout the tissue section. Their theoretical and observed monoisotopic mass values are listed in Table S1. Other phosphatidylethanolamines like PE(34:3), PE(36:6), PE(38:6), and PE(P-38:5) were found intensely distributed within the head and thorax region of *An. stephensi* (Figure 3, Figure 4, and Table S1). Two other phosphatidylethanolamines, PE(36:1) and PE(40:7), were predominantly found in the head and antennal lobe of the mosquito. Ether-linked PEs were observed especially in the head (Figure 5), among which PE(O-38:4) was found to be more abundant than PE(O-36:3) (Table S1). Ether linked PEs were also found in the homogenized samples of *Drosophila* heads, by using high-resolution mass spectrometry.[22]

Lysophosphatidylethanolamines. Lysophosphatidylethanolamines (LPEs) are enzymatic breakdown products of PEs, found to be spatially distributed in the head, thorax, and epithelium of the whole gut region of the mosquito (Figure 6). LPEs are minor constituents of cell membranes that play a role in cell-mediated cell signaling and activation of other enzymes.[23] They furthermore have been shown to have antifungal and antibacterial activity in the housefly.[24] We found a similar distribution of LPE(16:1) and LPE(18:1) in the head, thorax, and epithelium of the whole midgut (Figure 6),

with the intensity of LPE(16:1) being higher than that of LPE(18:1) (Table S1).

Phosphatidic Acids and Lysophosphatidic Acids. Phosphatidic acids (PAs) are involved in membrane biosynthesis and signal transduction in eukaryotes and emerged as key molecules in cellular signaling and trafficking.[25] Elevated levels of PAs were observed in dengue virus-infected mosquito cells[26] and *Plasmodium*-infected erythrocytes.[9] PA(38:4) and PA(38:6) were detected in the whole body of *An. stephensi* (Figure 3 and Table S1). Lysophosphatidic acids LPA(16:0), LPA(20:3), and LPA(20:4) were found to be localized in the head and thorax (Figure 4 and Table S1), whereas the prominent location of LPA(18:2) and LPA(20:2) was observed in the head, thorax, and whole gut epithelial region of *An. stephensi* (Figure 6 and Table S1).

Phophatidylglycerols. Phophatidylglycerols (PGs) were found only in lower amounts in the mosquito. Among the PGs, PG(34:1), PG(36:4), and PG(38:5) showed similar distributions in the thorax and gut regions (Figure 6c and Table S1) while PG(38:2) was mainly found in the head and the gut (Figure 6b and Table S1).

Phophatidylinositols. Phosphatdylinositols (PIs) are another class of lipids detected in positive-ion mode in the whole body and the head of *An. stephensi*. Plasmalogens are typical brain and muscle phospholipids. The similarity of distributions of plasmalogen PI(P-34:2) and PI(P-34:3) is shown in Figure 3, differing slightly in their relative intensities (Table S1). PI(36:3) showed up only in the head of the mosquito (Figure 5).

Sphingolipids. Sphingolipids act as second messengers by transducing signals between cellular compartments and regulating differentiation and apoptotic events in insects.[27] It has also been reported that various pathogens, including *Plasmodium*, require sphingolipids of host cells for infection.[28] An enhanced understanding of the sphingolipid utilization by

Plasmodium and a disruption of this metabolic route might provide possible targets for the treatment of malaria.

The positive-ion AP-SMALDI images of the sphingomyelins SM(34:1) and SM(36:1) indicate that they are similarly and uniformly distributed throughout the head and gut regions of the mosquito (Figure 6b and Table S1). The on-tissue MS/MS analysis of the potassiated SM(34:1) precursor ion at *m/z* 741.552931 expressed the fragment ion peak at *m/z* = 682.45645, which evolved from a neutral loss of 59 u, corresponding to trimethylamine, $(CH_3)_3N$, which is a diagnostic fragment ion for both PC and SM, since they share a similar headgroup.[29] Another prominent product ion peak at *m/z* = 162.95561 was assigned a signature fragment ion from the potassiated headgroup of phosphatidylcholines or sphingomyelins (Figure S3). It had been assumed for a long time that *Diptera* lack sphingomyelins but contain the related ceramide phosphoethanolamine instead.[30] However, sphingomyelins have been observed in *Manduca sexta* and are thought to be components of lipid rafts, plasma membrane microdomains enriched in sphingolipids and cholesterol.[31] Here we could identify sphingomyelins in *An. stephensi*.

Ceramide Phosphoethanolamines. Ceramide phosphoethanolamines (Cer-PE), which are preferentially expressed in insect cells,[31] have also been observed in this MSI study. Figure 5 shows a similar distribution of Cer-PE(34:1), Cer-PE(36:1), and Cer-PE(38:1), differing slightly in their intensities (Table S1).

■ ANATOMICAL REGIONS

Whole-Body Appearance of Phospholipids. Four major classes of phospholipids, phosphatidic acids (PAs), phosphatidylcholines (PCs), phosphatidylethalomines (PEs), and phosphatidylinositols (PIs), were found throughout the whole-body section and were assigned within a mass accuracy of ±1 ppm (Table S1). PCs, PAs, and PEs were found to be abundant in the whole section, in contrast to less abundant PIs. Lipid species distributed in the whole body of the mosquito are displayed in Figure 3. A total of 16 phospholipid species were determined to be distributed all over the *Anopheles* anatomy and were assigned according to protonated, sodiated, and potassiated species signals. Ion signals corresponding to PCs were found to be most abundant, ranging in total fatty acyl chain lengths of 32−36 carbon atoms (Figure S1). In the whole body of the mosquito, the less abundant PIs were detected in the form of plasmalogens (Table S1 and Figure 3).

Predominant Appearance in the Head and Thorax. Nine phospholipid species were selected in Figure 4 as being specifically abundant in the head and the thorax of the mosquito (Table S1). In these regions, enzyme-catalyzed lysolipids were found to be prominently concentrated, including lysophosphatidic acids, LPAs (16:0, 20:3, 20:4), and lysophosphatidylcholines, LPCs (16:0, 18:3). The next abundant lipids were found to be phosphatidylethanolamines, PEs (36:6, 38:6 and plasmalogen 38:5), and a saturated phosphatidylcholine, PC (32:0) (Figure 4).

Predominant Appearance in the Head and Antennal Lobe. The head and antennal lobe of *Anopheles* were found to be characterized by intense signals of sphingolipids and ether phospholipids, with an overall carbon length of 34−38, such as ceramide-phosphatidylethanolamines and ether-phosphatidylethanolamines. Ceramide phosphoethanolamines (Cer-PE) are known to be preferentially expressed in insect cells.[10] Ion signals of several unsaturated CerPEs (34:1, 36:1, and 38:1)

and ether PEs (36:2, 36:3, and 38:4) were found enriched in the head and antennal lobe of this female mosquito. The identity of these ether lipids was previously verified in homogenized samples of *Drosophila* heads by coupling on-column extraction (OCE) and liquid chromatography/multi-stage mass spectrometry.[32] Other lipid species found similarly distributed were saturated LPC(18:0) and unsaturated PE(40:7). In total, 8 phospholipid species were detected and assigned with a mass accuracy of 2 ppm (Table S1). Images of brain-specific phospholipids explored by AP-SMALDI-MSI are collected in Figure 5.

Predominant Appearance in the Head, Thorax, and Gut Epithelium. Distinct topographic patterns of 6 enzyme-catalyzed lysophospholipids, found concentrated in the head, thorax, and gut epithelium of *Anopheles* in the acyl chain carbon lengths of 18−20 are shown in Figure 6A (Table S1). Lysophospholipids found similarly distributed within these regions were unsaturated LPCs (18:1, 20:4), LPAs (18:2, 20:2), and LPEs (16:1, 18:1). All of these lysolipids were found more intensely in the head and thorax than in the gut epithelium (Figure 6A).

Predominant Appearance in Head and Whole Gut. Five phospholipid species were found predominantly in the head and whole gut of the mosquito (Table S1). Among these, two major sphingolipids were found, sphingomyelins SM(34:1) and SM(36:1), showing particularly high ion signals in the head compared to the whole gut (Figure 6B). Three other lipids with similar spatial distributions were PA(38:3), PC(36:1), and phosphatidyglycerol PG (38:2) (Figure 6B). PGs are typically detected in negative-ion mode due to their negatively charged headgroup. Here we detected sodium and potassium adducts of PGs in the positive-ion mode.

Predominant Appearance in Thorax and Whole Gut. Three potassium and sodium-attached phosphatidylglycerols PGs (34:1, 36:4, 38:5) were found to be predominantly located in the thorax and whole gut of *Anopheles* (Figure 6C). No signals of these phosphatidylglycerols were found in the head of the mosquito.

■ CONCLUSIONS

Our results indicate that AP-SMALDI-MSI provides high-quality molecular images obtained from insect tissue sections with high performance both in spatial resolution and mass resolution. Unique and specific spatial distributions of lipid species were observed by AP-SMALDI mass spectrometry imaging from *An. stephensi* tissue sections. This first approach of mosquito imaging revealed the location of many different lipids including glycerophospholipids, sphingolipids, and glycerolipids (data not shown). The relative abundance of these lipids can be estimated based on the intensities of their observed quasimolecular ion signals belonging to the same phospholipid compound.

Despite an increasing interest in the role of lipids in host−pathogen interactions, the number of studies addressing the lipid profile of insects, which serve as vectors for pathogenic diseases, remains low. So far the cuticle lipid profile of several *Anopheles* species has been investigated, however, with an emphasis on species discrimination or pheromone identification.[33,34] To our best knowledge, our study is the first whole-body mapping of lipids of *Anopheles* mosquitoes. A dedicated preparation method for analyzing *Anopheles* and other insect tissue was an important basis for these results, enabling intact cryo-preserved tissue sections from whole insects after CMC

embedding. This novel approach employing high-performance AP-SMALDI-MSI has great potential to support future studies of the pathophysiology of malaria by investigating changes in the molecular composition of host tissues induced by *Plasmodium* infection, parasite–host interactions, and drug discovery approaches. Further comparative analyses of *Plasmodium*-infected versus noninfected *An. stephensi* are underway to reveal changes in the lipid pattern after malaria infection.

■ ASSOCIATED CONTENT

Supporting Information

The Supporting Information is available free of charge on the ACS Publications website at DOI: 10.1021/acs.analchem.5b02781.

  Additional experimental details, mass spectra, and mass spectral data (PDF)

■ AUTHOR INFORMATION

Corresponding Author

*Phone: +49-641-9934800. Fax: +49-641-9934809. E-mail: bernhard.spengler@anorg.chemie.uni-giessen.de.

Notes

The authors declare no competing financial interest.

■ ACKNOWLEDGMENTS

■ REFERENCES

(1) Spengler, B. *Anal. Chem.* **2015**, *87*, 64–82.
(2) Chughtai, K.; Heeren, R. M. A. *Chem. Rev.* **2010**, *110*, 3237–3277.
(3) Goto-Inoue, N.; Yamada, K.; Inagaki, A.; Furuichi, Y.; Ogino, S.; Manabe, Y.; Setou, M.; Fujii, N. L. *Sci. Rep.* **2013**, *3*, 3.
(4) Römpp, A.; Spengler, B. *Histochem. Cell Biol.* **2013**, *139*, 759–783.
(5) *World Malaria Report 2013*, World Health Organization, 2013, ISBN 978-92-4-156469-4.
(6) Kai Wengelnik, V. r. V.; Ancelin, M. L.; Anne-Marie Cathiard, J. L. M.; Kocken, C. H.; Miche le Calas, S. H.; Thomas, A. W.; Vial, H. J. *Science* **2002**, *295*, 1311–1314.
(7) Schwartz, R. S.; Olson, J. A.; Raventos-Suarez, C.; Yee, M.; Heath, R. H.; Lubin, B.; Nagel, R. L. *Blood* **1987**, *69*, 401–407.
(8) Fuchs, B.; Schiller, J. *Mini-Rev. Med. Chem.* **2009**, *9*, 368–378.
(9) Vial, H. J.; Eldin, P.; Tielens, A. G. M.; van Hellemond, J. J. *Mol. Biochem. Parasitol.* **2003**, *126*, 143–154.
(10) Nawabi, P.; Lykidis, A.; Ji, D.; Haldar, K. *Eukaryotic Cell* **2003**, *2*, 1128–1131.
(11) Koestler, M.; Kirsch, D.; Hester, A.; Leisner, A.; Guenther, S.; Spengler, B. *Rapid Commun. Mass Spectrom.* **2008**, *22*, 3275–3285.
(12) Römpp, A.; Guenther, S.; Schober, Y.; Schulz, O.; Takats, Z.; Kummer, W.; Spengler, B. *Angew. Chem., Int. Ed.* **2010**, *49*, 3834–3838.
(13) Guenther, S.; Römpp, A.; Kummer, W.; Spengler, B. *Int. J. Mass Spectrom.* **2011**, *305*, 228–237.
(14) Bhandari, D. R.; Schott, M.; Römpp, A.; Vilcinskas, A.; Spengler, B. *Anal. Bioanal. Chem.* **2015**, *407*, 2189–2201.

(15) Strohalm, M.; Strohalm, J. i.; Kaftan, F.; Krásný, L. s.; Volný, M.; Novák, P.; Ulbrich, K.; Havlíček, V. r. *Anal. Chem.* **2011**, *83*, 5458–5462.
(16) Niehoff, A.-C.; Kettling, H.; Pirkl, A.; Chiang, Y. N.; Dreisewerd, K.; Yew, J. Y. *Anal. Chem.* **2014**, *86*, 11086–11092.
(17) Bouschen, W.; Schulz, O.; Eikel, D.; Spengler, B. *Rapid Commun. Mass Spectrom.* **2010**, *24*, 355–364.
(18) Butters, T. D.; Hughes, R. C. *In Vitro* **1981**, *17*, 831–838.
(19) Marheineke, K.; Grünewald, S.; Christie, W.; Reiländer, H. *FEBS Lett.* **1998**, *441*, 49–52.
(20) Furt, F.; Moreau, P. *Int. J. Biochem. Cell Biol.* **2009**, *41*, 1828–1836.
(21) Gibellini, F.; Smith, T. K. *IUBMB Life* **2010**, *62*, spc1.
(22) Chintapalli, V. R.; Al Bratty, M.; Korzekwa, D.; Watson, D. G.; Dow, J. A. T. *PLoS One* **2013**, *8*, e78066.
(23) Gode, D.; Volmer, D. A. *Analyst* **2013**, *138*, 1289.
(24) Meylaers, K.; Clynen, E.; Daloze, D.; DeLoof, A.; Schoofs, L. *Insect Biochem. Mol. Biol.* **2004**, *34*, 43–49.
(25) Testerink, C.; Munnik, T. *J. Exp. Bot.* **2011**, *62*, 2349–2361.
(26) Perera, R.; Riley, C.; Isaac, G.; Hopf-Jannasch, A. S.; Moore, R. J.; Weitz, K. W.; Pasa-Tolic, L.; Metz, T. O.; Adamec, J.; Kuhn, R. J. *PLoS Pathog.* **2012**, *8*, e1002584.
(27) Acharya, U.; Acharya, J. K. *Cell. Mol. Life Sci.* **2005**, *62*, 128–142.
(28) Heung, L. J.; Luberto, C.; Del Poeta, M. *Infect. Immun.* **2006**, *74*, 28–39.
(29) Garrett, T. J.; Prieto-Conaway, M. C.; Kovtoun, V.; Bui, H.; Izgarian, N.; Stafford, G.; Yost, R. A. *Int. J. Mass Spectrom.* **2007**, *260*, 166–176.
(30) Wiegandt, H. *Biochim. Biophys. Acta, Lipids Lipid Metab.* **1992**, *1123*, 117–126.
(31) Abeytunga, D. T. U. *J. Lipid Res.* **2004**, *45*, 1221–1231.
(32) Hebbar, S.; Schulz, W. D.; Sauer, U.; Schwudke, D. *Anal. Chem.* **2014**, *86*, 5345–5352.
(33) Suarez, E.; Nguyen, H. P.; Ortiz, I. P.; Lee, K. J.; Kim, S. B.; Krzywinski, J.; Schug, K. A. *Anal. Chim. Acta* **2011**, *706*, 157–163.
(34) Caputo, B.; Dani, F. R.; Horne, G. L.; N'Fale, S.; Diabate, A.; Turillazzi, S.; Coluzzi, M.; Costantini, C.; Priestman, A. A.; Petrarca, V.; della Torre, A. *Insect Biochem. Mol. Biol.* **2007**, *37*, 389–398.